Low Temperature Physics/Fizika Nizkikh Temperatur, 2015, v. 41, No. 1, pp. 81–85

Medical applications of EPR

Uwe Eichhoff and Peter Höfer

Bruker BioSpin GmbH, Silberstreifen, D-76287 Rheinstetten/Germany
E-mail: Uwe.Eichhoff@bruker-biospin.de

Received September 16, 2014, published online November 24, 2014

Selected applications of continuous-wave EPR in medicine are reviewed. This includes detection of reactive oxygen and nitrogen species, pH measurements and oxymetry. Applications of EPR imaging are demonstrated on selected examples and future developments to faster imaging methods are discussed.

PACS: **87.53.–j** Effects of ionizing radiation on biological systems;
87.64.kh EPR.

Keywords: EPR, reactive oxygen and nitrogen species, EPR dosimetry, oxymetry, EPR imaging.

Introduction

Electron paramagnetic resonance (EPR) was discovered 70 years ago by Zavoisky [1,2]. It relies on the resonance of an unpaired electron spin in the magnetic field, which limits its application to free radicals and transition metals. In contrary nuclear magnetic resonance (NMR) can be applied to all isotopes of chemical elements with a nuclear magnetic moment, that means to almost all elements of the periodic table [3]. Disregarding the limited objects of investigation EPR has found a large field of applications in almost any field of natural science and technology, especially in physics, chemistry, biology and medicine. A very good overview can be found in the book of K.M. Salikhov [4,5]. The opening of EPR to new applications was due to three main developments: transient and pulse EPR [6], high-field EPR [7–9] and the introduction of spin labels [10] and spin traps [11]. Most applications in biology, biochemistry are based on these compounds.

Reactive oxygen (ROS) and nitrogen species

EPR in medical and pharmaceutical investigations is based on the quantitative determination of free radicals in the organism, mainly of reactive oxygen species (ROS) and reactive nitrogen species (RNS) [12–14]. Reactive oxygen species like superoxide and hydroxide are formed by radiation or by malfunctions of some enzymes. They are often an indication of a pathological state. ROS normally have low concentration and short lifetime. Spin labels allow to add a paramagnetic center to the EPR-silent molecules and allow detection by EPR. Short-lived radicals can be caught by spin traps and form long living radicals, which then become also accessible to EPR. Antioxidant activity can be monitored through the reaction with diphenylpicrylhydrazine (DPPH) (Fig. 1(a)) and spin trapping with butyl-phenyl-nitron (PBN) (Fig. 1(d)). ROS are involved in aging [15], diabetes [16], hypertension [17], cardiovascular diseases [18], infections and inflammations [19], Alzheimer disease [20], lung disease [21] and cancer. Their concentration in blood plasma is increased by stress but can be diminished by physical exercise [22] (Fig. 2). For instance, players of Bavaria Munich EPR showed an increase of ROS by 40% after a soccer game.

The NO-radical, which is involved in many processes in the organism, can be detected directly. Peroxynitrite gives

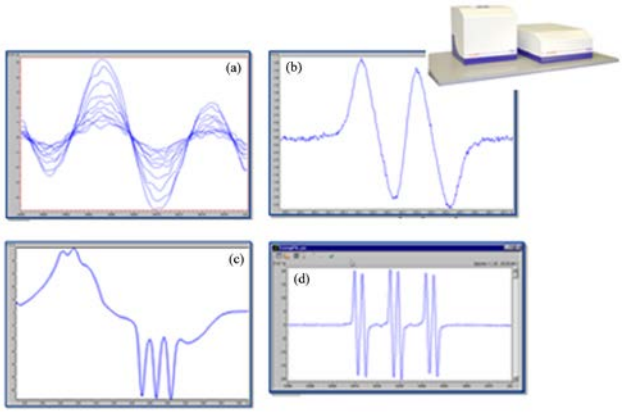

Fig. 1. (Color online) EPR measurements of reactive oxygen and reactive nitrogen species: (a) DDPH assay. DDPH is attacked by ROS. DPPH signal is inversely proportional to ROS concentration; (b) Oxidation leads to ascorbyl radical. Ascorbyl signal is proportional to ROS concentration; (c) NO bound to hemoglobin at 77 °C (finger dewar); (d) Spin trapping of ROS by PBN.

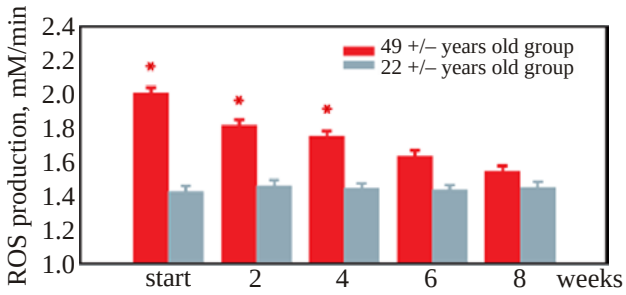

Fig. 2. (Color online) ROS production profile in human volunteers during moderate daily exercise for 8 weeks. Elder people have higher ROS blood level then young ones, but they can decrease it by exercise, whereas for younger people the low level remains almost constant.

no EPR signal, but forms with the reactive oxygen species EPR active long living nitroxyl radicals. Nitric oxide binds to hemoglobin forming a long living spin-labeled adduct with is detectable at low temperature and allows to determine the NO concentration in blood plasma (Fig. 1(d)).

Measurements of ROS and RNS must be performed at clearly defined temperature and oxygen partial pressure.

pH measurements

One of the key biological parameters in the maintenance of physiological homeostasis is pH. The EPR spectra of some radicals are sensitive to pH. The hyperfine coupling (hfc) is altered by pH of the local environment. By acquiring hfc measurements across a range of known pH samples, a calibration curve (hfc vs known pH) can be constructed. The pH can be even used as an imaging parameter. In cancer research extracellular pH (pHe) may provide a useful biomarker for tumor cell metabolism. The hfc of a pH-sensitive nitroxide (R-SG) was measured in a mouse cancer model before and after x-ray irradiation. During growth the tumor tissue becomes more acidid. After irradiation the tumor growth is stopped and the pH goes back to its initial value (Fig. 3).

Effects of ionizing radiation, EPR dosimetry

Ionizing radiation leads to disruption of chemical bonds and formation of free radicals. The amplitude of the corresponding EPR signal is over a wide range proportional to the radiation dose [24–26]. In the regions, which suffered from the Chernobyl accident in Russia, Belorussia and Ukraine, EPR spectrometry is used for tooth enamel dosimetry [27–29]. The EPR signal of tooth enamel reflects the total radiation dose, which a person has accumulated during its life (Fig. 4). EPR spectrometers for these investigations need a very high sensitivity and stability.

EPR imaging

Any EPR spectrometer can be extended to EPR imaging by adding gradient coils with a special power supply and appropriate software. For medical applications the strong absorption by water in the X-band is an additional obstacle. Biological objects due to their greater size and high water content are therefore better investigated in the L- and S-bands with a special large bore magnet and gradient assembly. For material science X- and Q-bands are preferable due to higher sensitivity. A standard universal EPRI system includes two magnet systems for X- and L-bands. Human whole-body EPR imaging like with NMR is in principle possible, but only with very low sensitivity and extremely long imaging times at very low frequencies in the MHz range. This fact additionally to the low radical concentration in the organism prevents its clinical application.

Additionally, in contrary to MRI, EPR imaging relies mainly on continuous wave (cw) methods. The short relaxation times in EPR (nsec–μsec), further shortened by the strong imaging gradients, do not allow to apply pulse sequences and Fourier imaging, which are standard in

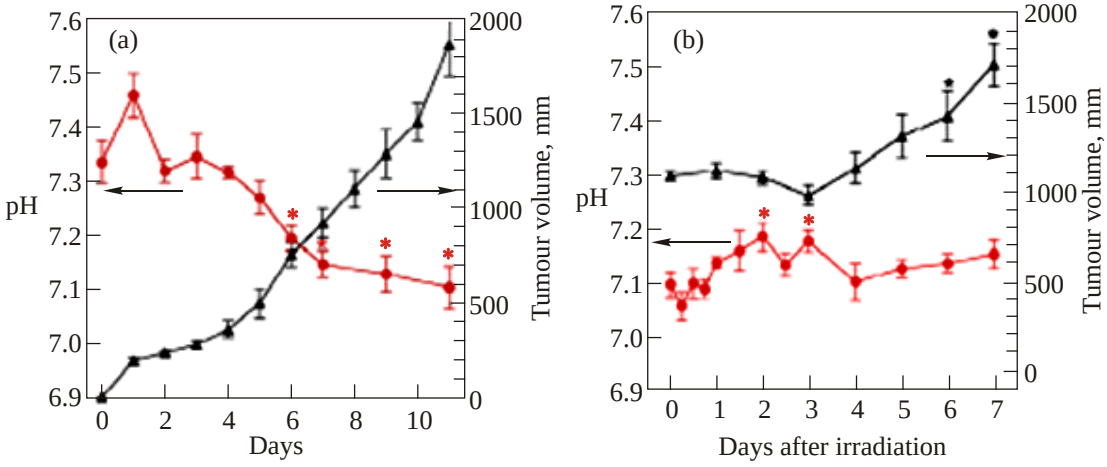

Fig. 3. (Color online) Relationship between tumor volume and pHe during normal tumor growth. An inverse relationship between tumor volume and pHe was observed in all mice from Day 3. Significant difference in pHe between Day 0 and Day *N* is shown "*" (Fig. 3(b)) tumour regrowth and pHe in irradiated mice.

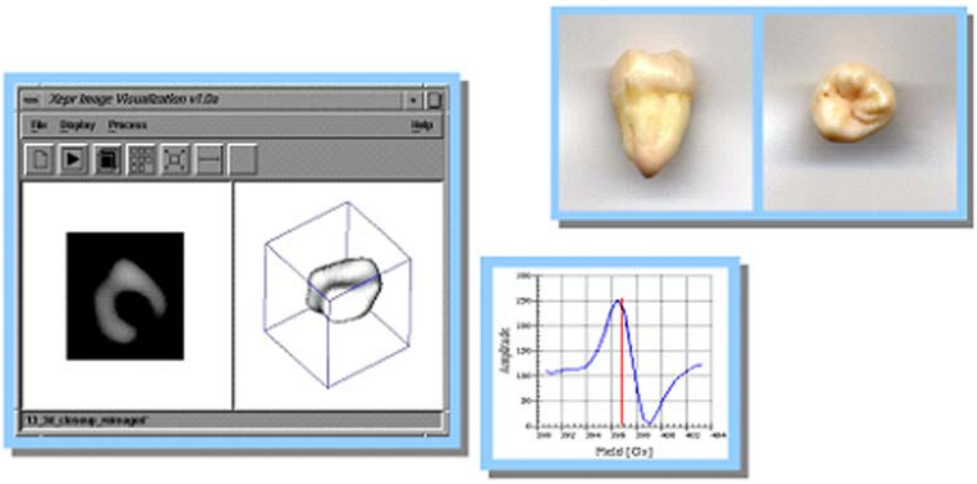

Fig. 4. (Color online) Irradiation-induced defects in teeth. Human upper 3rd molar (wisdom tooth) after x-ray irradiation: EPR signal at $g = 2$ line width ≈ 0.2 mT. The EPR image shows radiation-induced radicals mainly on the surface in the tooth-enamel. This is the basis of tooth-enamel dosimetry, which allows to determine the total radiation a person has received during his life-time. (Data courtesy of Dr. Graham Timmins, University of Wales College of Medicine, Cardiff, UK.)

MRI [30]. Therefore at present the EPR cw spectrum is measured in the presence of a gradient, which is stepped in two or three coordinate directions and the image is obtained by back-projection like in x-ray tomography and in the very early days of MRI.

In EPR imaging the relationships between field of view (FOV), spatial resolution, pixel bandwidth and gradient strength are the same as for MRI. In practice, however, there is a large difference regarding the pixel bandwidth. In low and medium field MRI the gradient strength is often large enough to ensure that no chemical shift distortion appears in the image. In EPRI suppression of hyperfine interaction in any image would require enormous gradients. Instead, the distortion of the spectral features by the gradient is removed using deconvolution with the original EPR spectrum yielding the integral EPR signal amplitude. For an EPR line width of 100 mG a resolution of 25 μ can be achieved.

One of the most promising applications of EPR imaging is oximetry [31,32]. The width of the EPR line depends on the partial oxygen pressure. The line width in blood can be calibrated against the partial oxygen pressure and then the partial oxygen pressure can be calculated from the EPR line width and displayed in a colour code. The image therefore reflects the oxygen concentration in the sample and ischemic conditions can be easily detected with EPR oximetry. An overlay on an MRI image relates the ischemic area to the anatomy (Fig. 5).

In malignant tumors like melanoma [33] radicals are created, which allow the imaging of core tumor and metastases. Melanin is an indogenous free radical responsible for the black pigments in melanoma. Ex vivo samples of melanoma have been imaged in the X-band with cw imaging (1024 points in 32.5 min). The comparison with the EPR images and the stained histological samples show a strong correlation between pigmentation and the EPR signal of melanin [34]. Unpigmented samples exhibit no EPR signal. EPR imaging of biopsies may evaluate stage and aggressiveness of melanoma. Figure 6 shows the melanin spectrum, 2D and 3D EPR images of melanoma in relation to histology and images of corresponding lung metastases.

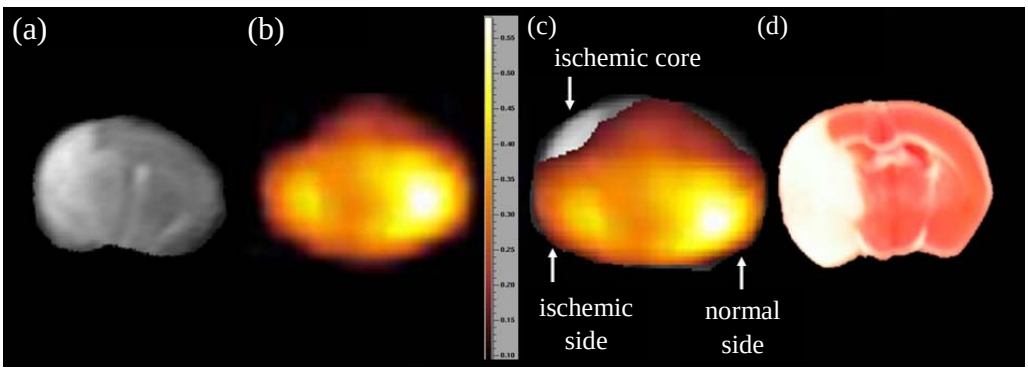

Fig. 5. (Color online) Ischemic stroke in rat brain: (a) MR diffusion image; (b) EPR line width image; (c) MRI/EPRI overlay; (d) histology.

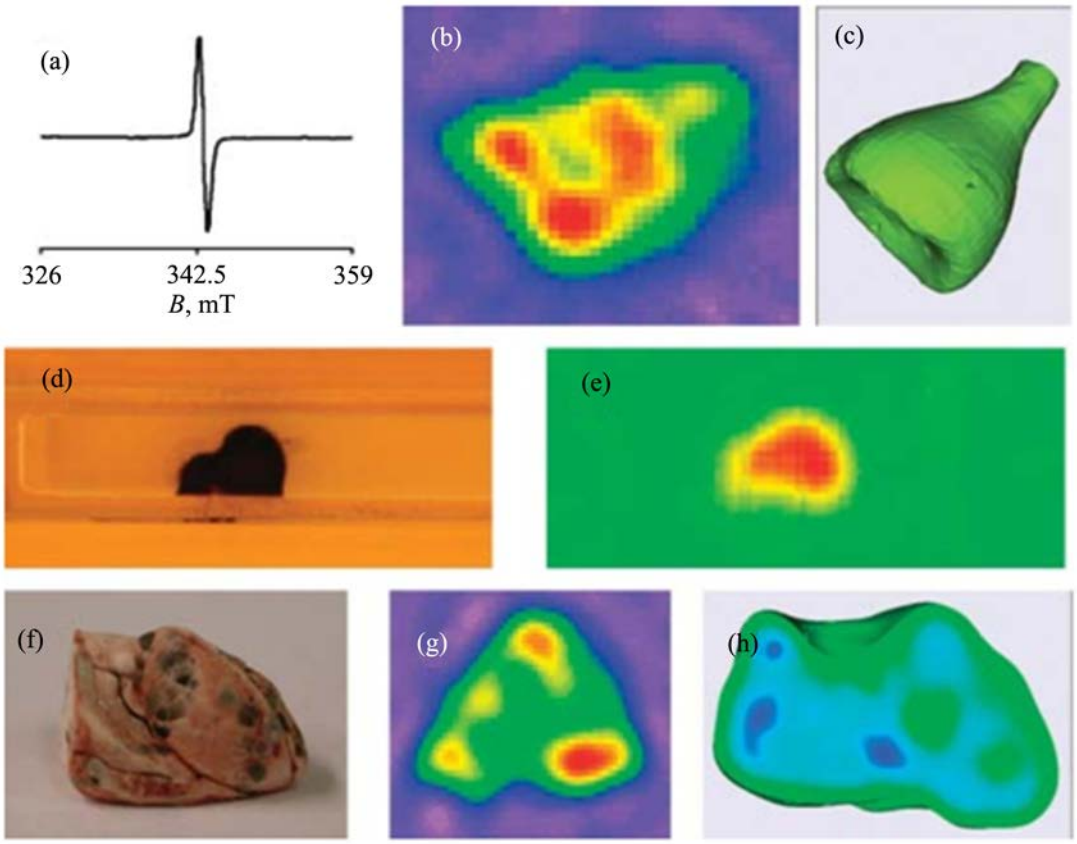

Fig. 6. (Color online) In vitro EPR spectra and images from melanoma B16 metastases in mice lung [1]: (a) spectrum from a freeze-dried melanoma; (b) 2D image; (c) 3D image; (d) picture from a fresh melanoma slice; (e) corresponding EPR image; (f) picture of freeze dried lungs with metastases; (g) 2D transversal EPR image; (h) longitudinal section through a 3D EPR image.

Pulse EPR, FT-EPR imaging

Pulse EPR, not only in imaging, meets many challenges. Relaxation times are in the range of nano- to microseconds (NMR: micro- to milliseconds). This necessitates fast digitizers and signal avaragers to detect the signals. This problem has been solved meanwhile with dwell times of 1 ns and even below. The signal to noise ratio (S/N) is proportional to the square root of the Q-factor and decays exponentially with the dead time t_d: $S/N \approx e^{-t_d/T_2} Q^{1/2}$. For sensitivity reasons it is desirable to have a high Q. But high Q leads to a small bandwidth and long dead time, during which the EPR signal may be significantly reduced or even vanish. The length of the exciting $\pi/2$ pulse is inversely proportional to the microwave power P: $t(\pi/2) \sim P^{-1/2}$ and must be in the order of the reciprocal line width to excite the broad EPR line. Therefore a compromise has to be made between the Q of the resonator and the dead time. As a rule of thumb the optimal Q is in the order of the relaxation time in nanoseconds (e.g., $Q = 100$ for $T_2 = 100$ ns). Therefore for most samples we have no sensitivity gain for pulsed EPR as compared to continuous wave.

These limitations are even more severe for pulse Fourier EPR imaging because the gradients cause additional line broadening. EPR imaging in cw mode is very time consuming. Modification of the single point imaging technique by compressed sensing and partial FT may lead to a significant reduction of imaging time (e.g., from 30 to 5 min) but cannot really access the short imaging times available in MRI.

Fourier EPR imaging is only possible for long relaxation times (or very narrow lines) resulting in imaging times well below one minute (Fig. 7). Rapid scan methods without field modulation may be a promising alternative [9,35,36] for broader lines. Scan rates above 13.4 kHz over a range

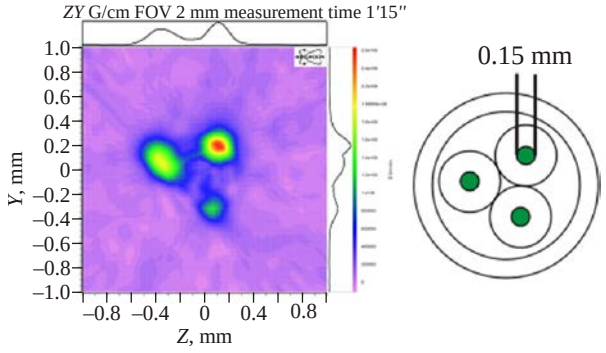

Fig. 7. (Color online) FT-EPR image of 3 trityl sample tubes (line width 0.3 MHz; left tube inclined, lower tube leaky) obtained with 32 ns-pulses in 12.7 s acquisition time (total imaging time including gradient recovery: 45 s).

of 155 G, sufficient for almost all radicals of medico-biological interest, have been achieved in a Bruker Flexline ER4118-XMD5 dielectric resonator (*Q*: 9000) over 150 G line width and increased sensitivity by one order of magnitude as compared to cw methods [37]. We believe, that the application of these methods to EPR imaging is just a matter of time.

1. E.K. Zavoisky, *Zh. Eksp. Teor. Fiz.* **15**, 344 (1944).
2. E.K. Zavoisky, *J. Phys*. **9**, 211 (1944).
3. R.K. Harris and B.E. Mann, *NMR and Periodic Table,* Academic Press (1978).
4. *The Treasures of Heureka,* Vol. I*: Electron Paramagnetic Resonance from Fundamental Research to Pioneering Applications & Zavoisky Award*, K.M. Salikhov (ed.), AXAS Publishing Ltd., New Zealand (2009).
5. S.S. Eaton, G.R. Eaton, and K.M. Salikhov, *Foundations of Modern EPR*, World Scientific, Singapore–New Jersey–London–Honkong (1998).
6. A. Schweiger and G. Jeschke, *Principles of Pulse Electron Paramagnetic Resonance*, Oxford University Press, Oxford, New York (2001).
7. Ya.S. Lebedev, in: *Modern Pulsed and Continuous Wave Electron Spin Resonance,* L. Kevan and M.K. Bowman (eds.), Chap. 8: *High-Frequency Continuous Wave Electron Spin Resonance,* Wiley, New York (1990).
8. K. Möbius, A. Savitsky, and M. Fuchs, in: *Very High-Frequency ESR/EPR*, O.A. Grinberg and L.J. Berliner (eds.), Chap. 3: *Primary Processes in Photosynthesis. What do we Learn from High-Field EPR Spectroscopy?*, Kuwer, New York (2004).
9. S.S. Eaton, R.W. Quine, M. Tseitlin, D.G. Mitchell, G.A. Rinard, and G.R. Eaton, in: *Handbook of High-Frequency EPR*, S. Misra (ed.), Wiley, New York (2014).
10. L.J. Berliner, *Spin Labeling II: Theory and Applications*, Academic Press, New York (1979).
11. E.G. Janzen, *Methods Enzymol*. **105**, 188 (1984).
12. D.G. Harrison and S. Dikalov, in: *Molecular Mechanisms in Hypertension Abington*, D. DiPette, E. Schiffrin, and E. Sowers (eds.), U.Uk., Taylor & Francis Medical Books (2006), p. 297.
13. H. Shi, G. Timmins, M. Monske, A. Kalyanamaran, Y. Liu, J.L. Clement, S. Burchiel, and K.J. Liu Arch, *Bichem. Biophys*. **471**(1), 437 (2005).
14. S. Dikalov, M. Skatchkov, and E. Basenge, *Biochem. Biophys. Res. Commun*. **231**, 701 (1997).
15. D.S. Erdincler, A. Seven, F. Inci, T. Beger, and G. Candan, *Clin. Chim. Acta* **265,** 77 (1997).
16. T.J. Guzik, S. Mussa, D. Gastaldi, J. Sadowski, C. Ratnatunga, R. Pillai, and K.M. Channon, *Circulation* **105**, 1656 (2002).
17. M.C. Gongora, Z. Quin, K. Laude, H.W. Kim, L. McCann, J.R. Folz, S. Dikalov, T. Fukai, and D.G. Harrison, *Hypertension* **48**, 473 (2006).
18. S. Dikalov, K.K. Griendling, and D.G. Harrison, *Hypertension* **49**, 1 (2007).
19. G.M. Rosen, B.E. Britigan, H.J. Halpern, and S. Pou, in: *Free Radicals, Biology and Detection by Spin Trapping*, Oxford Univeristy Press, New York (1999).
20. J. Petrlova, T. Kalai, I. Maezawa, R. Altman, G. Harishandra, H.S. Hong, D.A. Bricarello, A.N. Parikh, G.A. Lorigan, L.W. Jin, K. Hideg, and J.C. Voss, *Plos One* 7 (4), e35443 (2012). doi:10.1371/journal.pone.0035443.
21. N.W. Kooy, J.A.A. Royall, Y.Z. Ye, D.R. KJelly, and J.S. Beckman, *Am. J. Respir. Crit. Care Med*. **151**, 1250 (1995).
22. M.I. Covas, R. Elosua, M. Fito, M. Alcantara, L. Coca, and J. Marrugat, *Med. Sci. Sports Exerc.* **34,** 814 (2002).
23. J. Goodwin, K. Yachi, M. Nagane, H. Yasui, Y. Miyake, O. Inanami, A.A. Bobko, V.V. Khramtsov, and H. Hirata, *Proc. Intl. Soc. Mag. Reson. Med*. **22**, 2932 (2014).
24. D.F. Ragulla and U. Deffner, *Appl. Radiat. Isotopes* **33**, 1101 (1982).
25. H. Ishii and M. Ikeya, *Jpn. J. Appl. Phys.* **29**, No. 5, 871 (1990).
26. M.A. Brilliant et al., *Hematologia and Transfusiologia* **9**, 14 (1990).
27. M. Ikeya, *Magn. Reson. Rev.* **13**, No. 3, 91 (1988).
28. B. Pass and J.E. Aldrich, *Med. Phys.* **12**, No. 3, 305 (1985).
29. V.G. Skvortsov, A.I. Vannikov, and U. Eichhoff, *J. Mol. Struct.* **347**, 321 (1995).
30. A. Kumar, D. Welti, and R. Ernst, *J. Magn. Reson*. **18**, 69 (1975).
31. M. Elas, B.B. Williams, A. Parasca, C. Mailer, C.A. Pelizzari, M.A. Lewis, J.A. River, G.S. Karczmar, E.D. Barth, and H.J. Halpern, *Magn. Reson. Med.* **49**, 682 (2003).
32. M. Elas, K.-H. Ahn, A. Parasca, E.D. Barth, D. Lee, C. Haney, and H.J. Halpern, *Clin. Cancer Res.* **12**,4209 (2006).
33. E. Vanea, N. Charlier, J. DeWever, M. Dinguizli, O. Feron, J.F. Baurain, and B. Gallez, *NMR Biomed.* **21**, 296 (2008).
34. Q. Godechal, G. Ghanem, M. Cook, and B. Gallez, *Proc. Intl. Soc. Mag. Reson. Med*. **21**, 1988 (2013).
35. D.G. Mitchell, R.W. Quine, M. Tseitlin, S.S. Eaton, and G.R. Eaton, *J. Magn. Reson*. **214,** 221 (2012).
36. D.G. Mitchell, G.M. Rosen, M. Tseitlin, B. Symmes, S.S. Eaton, and G.R. Eaton, *Biophys. J.* **105**, 338 (2013).
37. Yu. Zhelin, R.W. Quinn, G.A. Rinard, M.Tseitlin, H. Elajaili, V. Kathirvelu, L.J. Clouston, P.J. Boratynski, A. Rajca, R. Stein, H. Mchaourab, S.S. Eaton, and G.R. Eaton, *submitted to J. Magn. Reson.* (2014).